A99-33539

AIAA 99-3348

Comparative Study of Upwind Scheme Performance for Entropy Condition and Discontinuities

Ge-Cheng Zha*
GE Aircraft Engines, Mail Drop 34044
Advanced Engineering Programs Dept.
1000 Western Avenue, Lynn, MA 01910
E-mail: gecheng.zha@ae.ge.com

Abstract

The upwind schemes of Roe, Van Leer, Steger-Warming, Van Leer-Hänel, Liou's AUSM and AUSM$^+$, Edwards LDFSS and modified Zha-Bilgen scheme are tested for their performance at sonic point and discontinuities. A numerical test case is presented to examine the entropy condition of upwind schemes at sonic point for nonlinear Euler equations. The Zha-Bilgen flux vector splitting scheme is modified to resolve contact discontinuities. It is observed that the schemes of Van Leer, Van Leer-Hänel, AUSM and AUSM$^+$ schemes allow expansion shock at sonic point. Two shock tube problems, the Sod problem and a slowly moving contact discontinuity, are also tested for these schemes. The focus for shock tube tests is on comparing the maximum allowable CFL number and the quality of the discontinuities captured. Edwards' LDFSS(2) scheme gives the best results at both sonic point and discontinuities.

* Lead Engineer, AIAA Member

1 Introduction

To treat the flows with shock waves and contact discontinuities, an accurate and efficient upwind scheme used as a Riemann solver to resolve the discontinuities is essential. Such an upwind scheme is particularly important when it is incorporated into a high order accuracy scheme such as an ENO scheme to simulate turbulence or acoustic fields with discontinuities, where the nonphysical noise should be minimized and the number of mesh points would be limited due to the computing power.

To achieve the purpose of efficiency and accuracy, efforts have been made to develop an upwind scheme only using scalar dissipation instead of using matrix dissipation such as that of Roe's flux difference splitting (FDS) scheme [1]. The modification of Van Leer's Flux Vector Splitting(FVS) scheme[2] by Hänel in 1987[3] began a series of new developments. The advection upstream splitting method(AUSM) suggested by Liou and Steffen [4] in 1993 has achieved high accuracy and maintained the computing work as low as that of the Van Leer scheme. Zha and Bilgen suggested a low diffusion Flux Vector Splitting

(LDFVS) scheme in 1993 [5], which may resolve crisp shock profile, but the contact discontinuity would be smeared. The Zha-Bilgen scheme has been modified to accurately resolve contact discontinuities in this paper. Jameson suggested his Convective Upwind and Split Pressure (CUSP) schemes and limiters in 1993, which may capture crisp shock profiles, but not contact discontinuities [6, 7, 8]. Liou's AUSM$^+$ scheme (1995) [9, 10] further improves the accuracy of AUSM scheme and is able to resolve the exact shock and contact discontinuities and preserve the constant total enthalpy for steady state flows. Using the similar concept to AUSM scheme, Edwards developed his low diffusion flux splitting scheme(LDFSS) in 1995 [11, 12]. The scheme shows the best performance in the numerical tests of this paper. The splitting formulations of Mach number and pressure from Van Leer's flux vector splitting scheme are employed in both AUSM and LDFSS schemes.

While progress has been made to reduce the dissipation of upwind schemes and improve their capability to capture discontinuities, relatively less attention has been paid to answer an important question: "Does the scheme satisfy the entropy condition?". For the FDS schemes such as the Roe's scheme [1] and Osher's scheme [13], it is known that the Roe scheme does not satisfy the entropy condition and the Osher scheme does. For the FVS schemes such as the Van Leer scheme and Steger-Warming scheme, it is not known whether they satisfy the entropy condition [14, 15]. The extensive and successful applications of the FVS schemes in practical computations lead to a general impression that a FVS scheme, in particular, the Van Leer scheme, is robust and violation of the entropy condition may not be an issue. However, this can not be served as the answer to the question raised above. For those recently developed schemes including AUSM family schemes, LDFFS schemes, CUSP schemes, and modified Zha-Bilgen scheme, etc, no definite answers are given regarding whether they satisfy the entropy condition. In general, some important numerical characteristics of the upwind schemes currently used are not fully understood.

The purposes of this paper are twofold: 1) to give a numerical test case which may answer the entropy condition question for some of the upwind schemes. If an upwind scheme generates an expansion shock, the scheme would be considered as violating the entropy conditions. If an upwind scheme does not generate an expansion shock for the test case, it is not conclusive that the scheme satisfies the entropy condition; 2)to compare the performance of those schemes to capture the shock and contact discontinuities. The interest is to compare the maximum allowable CFL numbers and the quality of the shock and contact discontinuities resolved.

To explore the original properties of the upwind schemes, the work in this paper mainly focuses on the 1D piece wise constant first order discretization.

2 Numerical Procedure

2.1 Governing Equations

The governing equations are the quasi-1D Euler equations in Cartesian coordinates:

$$\partial_t \mathbf{U} + \partial_x \mathbf{E} - \mathbf{H} = 0 \qquad (1)$$

where $\mathbf{U} = S\mathbf{Q}$, $\mathbf{Q} = \begin{pmatrix} \rho \\ \rho u \\ e \end{pmatrix}$, $\mathbf{E} = S\mathbf{F}$,

$$\mathbf{F} = \begin{pmatrix} \rho u \\ \rho u^2 + p \\ (e+p)u \end{pmatrix}, \text{ and } \mathbf{H} = \frac{dS}{dx} \begin{pmatrix} 0 \\ p \\ 0 \end{pmatrix}$$

In above equations, ρ is the density, u is the velocity, p is the static pressure, e is the total energy and S is the cross sectional area of the 1D duct. The following state equation is also employed:

$$p = (\gamma - 1)(e - \frac{1}{2}\rho u^2) \tag{2}$$

where γ is the specific heat ratio with the value of 1.4.

The finite volume method with the explicit Euler temporal integration is used to discretize the governing equations. It yields the following formulation at cell i:

$$\Delta \mathbf{Q}_i^{n+1} = \Delta t[-C(\mathbf{E}_{i+\frac{1}{2}} - \mathbf{E}_{i-\frac{1}{2}}) + \frac{\mathbf{H}_i}{S_i}]^n \tag{3}$$

where $C = 1/(\Delta x S_i)$, n is the time level index.

The following sub-sections list all the formulations of the different schemes used in this paper for the purpose of reproducing the results.

2.2 The Van Leer FVS Scheme[2]

The general form of the Van Leer FVS scheme is:

$$\mathbf{F}_{\mathbf{i+\frac{1}{2}}} = \mathbf{F}_{\mathbf{L}}^{+} + \mathbf{F}_{\mathbf{R}}^{-} \tag{4}$$

For subsonic flow, $|M| < 1$,

$$\mathbf{F}^{\pm} = \begin{pmatrix} f_m^{\pm} \\ f_m^{\pm} \frac{(\gamma-1)u \pm 2a}{\gamma} \\ f_m^{\pm} \frac{[(\gamma-1)u \pm 2a]^2}{2(\gamma^2-1)} \end{pmatrix} \tag{5}$$

where $f_m^{\pm} = \pm \rho a[\frac{1}{2}(|M| \pm 1)]^2$, a is the speed of sound and M is the Mach number.

For supersonic flow:

$$\mathbf{F}_{\mathbf{i+\frac{1}{2}}} = \mathbf{F}_{\mathbf{L}} \quad for \quad M_L > 1 \tag{6}$$

$$\mathbf{F}_{\mathbf{i+\frac{1}{2}}} = \mathbf{F}_{\mathbf{R}} \quad for \quad M_R < -1 \tag{7}$$

$$M_L = u_L/a_L, M_R = u_R/a_R$$

2.3 The Van Leer-Hänel Scheme[3]

The only difference between the Van Leer scheme and the Van Leer-Hänel Scheme is the energy term. The Van Leer-Hänel scheme can be expressed as the following:

$$\mathbf{F}_{\mathbf{i+\frac{1}{2}}} = \mathbf{F}_{\mathbf{L}}^{+} + \mathbf{F}_{\mathbf{R}}^{-} \tag{8}$$

For subsonic flow, $|M| < 1$,

$$\mathbf{F}^{\pm} = \begin{pmatrix} f_m^{\pm} \\ f_m^{\pm} \frac{(\gamma-1)u \pm 2a}{\gamma} \\ f_m^{\pm} h \end{pmatrix} \tag{9}$$

where $f_m^{\pm}$ is the same as defined in the Van Leer scheme, and h is the enthalpy evaluated as $h = \frac{e+p}{\rho}$.

For supersonic flow:

$$\mathbf{F}_{\mathbf{i+\frac{1}{2}}} = \mathbf{F}_{\mathbf{L}} \quad for \quad M_L > 1 \tag{10}$$

$$\mathbf{F}_{\mathbf{i+\frac{1}{2}}} = \mathbf{F}_{\mathbf{R}} \quad for \quad M_R < -1 \tag{11}$$

2.4 The Steger-Warming FVS Scheme[16]

The Steger-Warmimg FVS scheme is also written as:

$$\mathbf{F}_{i+\frac{1}{2}} = \mathbf{F}_{\mathbf{L}}^{+} + \mathbf{F}_{\mathbf{R}}^{-} \tag{12}$$

For subsonic flow, $0 < M < 1$,

$$\mathbf{F}^{+} = \frac{\rho}{2\gamma} \begin{pmatrix} 2\gamma u + a - u \\ 2(\gamma-1)u^2 + (u+a)^2 \\ (\gamma-1)u^3 + \frac{(u+a)^3}{2} + \frac{(3-\gamma)(u+a)a^2}{2(\gamma-1)} \end{pmatrix} \tag{13}$$

$$\mathbf{F}^{-} = \frac{\rho}{2\gamma} \begin{pmatrix} u - a \\ (u-a)^2 \\ \frac{(u-a)^3}{2} + \frac{(3-\gamma)(u-a)a^2}{2(\gamma-1)} \end{pmatrix} \tag{14}$$

For subsonic flow with $-1 < M < 0$, the formulation is not listed here but can be obtained symmetrically. For supersonic flow, it switches to fully one side flux as the Van Leer scheme.

2.5 The Liou's $AUSM^{+}$ scheme [10]

For $|M| < 1$:

$$\mathbf{F}_{i+\frac{1}{2}} = M_{\frac{1}{2}} a_{\frac{1}{2}} \frac{1}{2}(\psi_L + \psi_R) - \frac{1}{2} a_{\frac{1}{2}} |M_{\frac{1}{2}}| (\psi_R - \psi_L) + (\mathbf{P}_L + \mathbf{P}_R) \tag{15}$$

where $\psi = \begin{pmatrix} \rho \\ \rho u \\ \rho h \end{pmatrix}$, $\mathbf{P}_L = \begin{pmatrix} 0 \\ \mathcal{P}^{+} p_L \\ 0 \end{pmatrix}$, $\mathbf{P}_R = \begin{pmatrix} 0 \\ \mathcal{P}^{-} p_R \\ 0 \end{pmatrix}$,

$$M_{\frac{1}{2}} = \mathcal{U}^{+}(M_L) + \mathcal{U}^{-}(M_R)$$

$$\mathcal{U}^{\pm} = \pm\frac{1}{4}(M \pm 1)^2 \pm \beta(M^2 - 1)^2$$

$$a_{\frac{1}{2}} = min(\tilde{a}_L, \tilde{a}_R)$$

$$\tilde{a} = a^{*2}/max(a^*, |u|)$$

$$a^* = \sqrt{\frac{2(\gamma-1) * h}{(\gamma+1)}}$$

$$\mathcal{P}^{\mp} = \frac{1}{4}(M \pm 1)^2(2 \mp M) \pm \alpha M(M^2 - 1)^2$$

$$M_L = u_L/a_{\frac{1}{2}}, M_R = u_R/a_{\frac{1}{2}}$$

The α and β take the values suggested by Liou [10] as $\alpha = \frac{3}{16}$ and $\beta = \frac{1}{8}$.

2.6 The Modified Zha-Bilgen Scheme

The formulations of the Zha-Bilgen FVS scheme for subsonic flow [5] is modified to capture contact discontinuities by using the idea of an interface sound speed as suggested by Wada and Liou [17] for the pressure splitting. The formulation can be expressed as the following:

For $|M| < 1$:

$$\mathbf{F}_{i+\frac{1}{2}} = \frac{1}{2}(\mathbf{F_L} + \mathbf{F_R}) - \frac{1}{2}(\mathbf{D_R} - \mathbf{D_L}) \tag{16}$$

where $\mathbf{F}$ is defined as in eq. (1),

$$\mathbf{D} = |u|\mathbf{Q} + \begin{pmatrix} 0 \\ pM \\ pa_{\frac{1}{2}} \end{pmatrix} \tag{17}$$

$\mathbf{Q}$ is defined as in eq.(1)

$$a_{\frac{1}{2}} = \frac{1}{2}(a_L + a_R) \tag{18}$$

$$M_L = u_L/a_{\frac{1}{2}}, M_R = u_R/a_{\frac{1}{2}} \tag{19}$$

The interface speed of sound is essential for the scheme to resolve contact discontinuities.

For supersonic flow, it switches to fully one side flux as the Van Leer scheme. At the sonic point, the pressure splitting does not have a continuous derivative. If the switch Mach number M_L and M_R are simply determined as eq.(19), the computation is not able to drive the residual to machine zero. However, if the interface speed of sound, $a_{\frac{1}{2}}$, to determine the switch Mach number is computed by the procedure of AUSM$^+$ scheme, the residual can be reduced to machine zero with no difficulty. The same phenomenon also occurs to the Steger-Warming scheme. The machine zero herein is defined as the L2 Norm residual reduced by at least 12 orders of magnitude. This scheme has the simplest form among all the schemes tested.

2.7 The Roe FDS Scheme [1]

Roe's FDS scheme has a single formulation for both subsonic and supersonic flow :

$$\mathbf{F}_{i+\frac{1}{2}} = \frac{1}{2}(\mathbf{F_L} + \mathbf{F_R}) - \frac{1}{2}|\tilde{\mathbf{A}}|(\mathbf{Q_R} - \mathbf{Q_L}) \tag{20}$$

where $|\mathbf{A}| = \mathbf{T}|\mathbf{\Lambda}|\mathbf{T^{-1}}$,

$$\mathbf{T} = \begin{pmatrix} 1 & 1 & 1 \\ u-a & u & u+a \\ h-ua & \frac{1}{2}u^2 & h+ua \end{pmatrix}$$

and $|\mathbf{\Lambda}| = \begin{pmatrix} |u-a| & 0 & 0 \\ 0 & |u| & 0 \\ 0 & 0 & |u+a| \end{pmatrix}$.

The tilde $\tilde{}$ in eq. (20) means that all the elements of the matrix are evaluated by the following Roe's average [1]:,

$$\tilde{u} = \frac{\sqrt{\rho_L}u_L + \sqrt{\rho_R}u_R}{\sqrt{\rho_L} + \sqrt{\rho_R}}$$

$$\tilde{h} = \frac{\sqrt{\rho_L}h_L + \sqrt{\rho_R}h_R}{\sqrt{\rho_L} + \sqrt{\rho_R}}$$

$$\tilde{a} = (\gamma - 1)(\tilde{h} - \frac{1}{2}\tilde{u}^2)$$

2.8 Edwards LDFSS(2) scheme [11, 12]

Edwards LDFSS(2) scheme follows the similar methodology of AUSM family scheme, but has different splitting techniques.

$$\mathbf{F}_{i+\frac{1}{2}} = \mathbf{F}^c_{\frac{1}{2}} + \mathbf{F}^p_{\frac{1}{2}} \tag{21}$$

$$\mathbf{F}^c_{\frac{1}{2}} = a_{\frac{1}{2}}[\rho_L C^+ \tilde{\mathbf{F}}^c_L + \rho_R C^- \tilde{\mathbf{F}}^c_R] \tag{22}$$

where

$$a_{\frac{1}{2}} = \frac{1}{2}(a_L + a_R)$$

$$C^+ = \alpha^+_L(1+\beta_L)M_L - \beta_L M^+_L - M^+_{\frac{1}{2}}$$

$$C^- = \alpha^-_R(1+\beta_R)M_R - \beta_R M^-_R + M^-_{\frac{1}{2}}$$

$$M_L = \frac{u_L}{a_{\frac{1}{2}}}, M_R = \frac{u_R}{a_{\frac{1}{2}}}$$

$$\alpha^{\pm}_{L,R} = \frac{1}{2}[1 \pm sgn(M_{L,R})]$$

$$\beta_{L,R} = -max[0, 1 - int(|M_{L,R}|)]$$

$$\phi = \frac{(\rho a^2)_R}{(\rho a^2)_L}$$

$$M^+_{\frac{1}{2}} = M_{\frac{1}{2}} \frac{a_R + a_L\phi}{a_R + a_L}$$

$$M^-_{\frac{1}{2}} = M_{\frac{1}{2}} \frac{a_L + a_R/\phi}{a_R + a_L}$$

$$M_{\frac{1}{2}} = \beta_L \delta^+ M^-_L + \beta_R \delta^- M^+_R$$

$$M^{\pm}_{L,R} = \pm\frac{1}{4}(M_{L,R} \pm 1)^2$$

$$\delta^{\pm} = \frac{1}{2}(1 \pm sgn[1, \frac{1}{2}(M_L + M_R)]$$

$$\tilde{\mathbf{F}}^c = \begin{pmatrix} 1 \\ u \\ H \end{pmatrix}$$

$$\mathbf{F}^p_{\frac{1}{2}} = D^+_L \mathbf{p_L} + D^-_R \mathbf{p_R} \qquad (23)$$

$$D^{\pm}_{L,R} = \alpha^{\pm}_{L,R}(1 + \beta_{L,R}) - \beta_{L,R} P^{\pm}_{L,R}$$

$$P^{\pm}_{L,R} = \frac{1}{4}(M_{L,R} \pm 1)^2(2 \mp M_{L,R})$$

$$\mathbf{p} = \begin{pmatrix} 0 \\ p \\ 0 \end{pmatrix}$$

3 Results and Discussion

All of the following results were computed using first order accuracy unless specially indicated.

3.1 Test 1: Entropy condition

The test case is a simple quasi-1D transonic flow in a converging-diverging nozzle. The correct solution should be a smooth flow from subsonic to supersonic with no shock. However, for an upwind scheme which does not satisfy the entropy condition, an expansion shock may be produced. Since the purpose of this paper is not to cure the weakness of the upwind schemes tested, the remedies [18, 15] to consider the source terms and generalize those schemes are not explored in this paper.

3.1.1 Geometry

The geometry is one of a series of 2D converging-diverging nozzles designed and tested at NASA Langley Research Center[19], namely Nozzle A2 as sketched in Fig. 1. The geometry is formed by a plane upstream and downstream of the throat region with the slope angle of θ and β respectively. In the throat region, it has a circular-arc surface for transition. The geometry is symmetric about the central axis plane and only the upper half geometry is shown in the sketch (Fig. 1). The formulations describing the geometry are given below:

$$y = \tan(\theta)x + h_i, \quad for \quad 0 \le x \le L_1 \qquad (24)$$

$$y = -\sqrt{r_c^2 - (x - x_c)^2} + y_c, \quad for \quad L_1 \le x \le L_2 \qquad (25)$$

$$y = \tan(\beta)(x - x_t) + y_t, \quad for \quad L_2 \le x \le L_3 \qquad (26)$$

where $\theta = -22.33°, \beta = 1.21°$, $L_1 = 4.74cm, L_2 = 5.84cm, L_3 = 11.56cm$, $x_t =$

$5.84cm, y_t = 1.37cm, x_c = 5.78cm, y_c = 4.11cm$, $r_c = 2.74cm, h_i = 3.52cm$.

In the computation, the geometry is normalized by the half throat height $h_t = 1.37cm$.

3.1.2 Numerical Results

For the subsonic boundary conditions at the entrance, the velocity is extrapolated from the inner domain and the other variables are determined by the total temperature ($300K°$) and total pressure ($1013kPa$). For supersonic exit boundary conditions, all the variables are extrapolated from inside of the nozzle. The analytical solution was used as the initial flow field. The computation proceeded using a global time step in a time accurate fashion.

Fig. 2 is the comparison of the analytical and computed Mach number distributions with 201 mesh points using the schemes of Roe, Van Leer-Hänel, Liou's AUSM and AUSM$^+$ before these computations diverged. The schemes shown in Fig.2 were either not stable in time or diverged for mesh refinement. The analytical solution is smooth throughout and reaches the sonic speed at the throat (the minimum area of the nozzle, located at $X/h_t = 4.22$). It is seen that all these schemes generate expansion shocks at the nozzle throat location. The expansion shock of the Roe scheme had a large amplitude and was converged to machine zero with 201 mesh points and CFL=0.95. When a refined mesh with 401 points was used, the amplitude of the expansion shock generated by the Roe scheme largely oscillated in time and the calculation eventually diverged. The schemes of Van Leer-Hänel, Liou's AUSM and AUSM$^+$ were not stable even for 201 mesh points with CFL number lower than 0.1. The amplitude of the expansion shock generated by Van Leer-Hänel, Liou's AUSM and AUSM$^+$ schemes grew in time and the computation diverged soon after the results reached the state shown in Fig. 2 .

Fig. 3 is the Mach number distributions with 201 mesh points computed by the schemes of Van Leer, Steger-Warming, the modified Zha-Bilgen scheme suggested in section 2.6 and Edwards' LDFSS(2) scheme. All the results were converged to machine zero with CFL=0.95. It is seen that Van Leer scheme generates a strong expansion shock at the throat location. The derivatives of the modified Zha-Bilgen and Steger-Warming schemes are not continuous and there are small jumps at the sonic points as shown in the throat region. Edwards' LDFSS(2) scheme agrees the best with the analytical results with the least jump.

All the schemes in Fig. 3 produce results closer to the analytical one when the refined mesh with 401 points is used, as shown in Fig. 4. The amplitude of the expansion shock generated by the Van Leer scheme is also decreased with the refined mesh, but remains very large.

Van Leer indicated in [18] that the first order piece wise uniform value may not be a good representation of the solution near a sonic point for the schemes which do not satisfy the entropy conditions. It prevents the true gradient being computed at the sonic bordering zone and shows up as a transonic expansion shock. For a second order scheme, the expansion shock disappears or its amplitude reduces to $O[(\Delta x^3)]$(for Burgers' equation). Fig. 5 is the Mach number distributions for all the schemes using the second order MUSCL-type interpolation. It shows that all the schemes generate the solutions which are smooth and virtually identical to the analytical solution. The expansion shocks indeed disappear as analyzed by Van Leer[18]. This implies that it may be generally safe to avoid an

expansion shock as long as higher than first order MUSCL-type upwind differencing is used.

3.2 Test 2: Shock Tubes

The purpose here is to present the shock tube tests for different upwind schemes so that we can compare their performance. Two things are of interest to compare: 1) the maximum allowable CFL number to be used; 2) the quality of shock and contact discontinuities captured.

For the discontinuity quality, it is desired that they are crisp and monotone with no oscillation. For the maximum allowable CFL number with explicit Euler time integration, it is desired that the CFL number is as close to the upper limit of 1.0 as possible. For the 1D linear wave equation with CFL=1 and 1st order upwind scheme, the numerical dissipation and dispersion vanish [20]. For nonlinear Euler equations, it is also true that the closer the CFL to 1.0, the less the numerical dissipation, hence the sharper the discontinuity profiles captured.

3.2.1 Case 1: The Sod Problem

Fig. 6 to 12 are the computed temperature distributions compared with analytical results for the Sod problem [21] using 201 mesh points. They are listed in the order of maximum allowable CFL number magnitude from the largest to the smallest. The maximum allowable CFL number is defined as the number, beyond which the numerical solution will generate oscillation or become unstable. Edwards' LDFSS(2) scheme has the largest maximum allowable CFL number of 0.999 as shown in Fig. 6. The shock profile is sharp and monotone. The contact discontinuity is smeared, but it may be the sharpest profile that a first order scheme can achieve. The front of the expansion wave (located at about X/L=3.5) is also smeared. Overall, the computed results agree excellently with the analytical results.

Van Leer-Hänel scheme has the maximum CFL =0.99 and the whole profile is quite similar to the one of LDFSS(2) (see Fig. 7). The Steger-Warming scheme has the maximum CFL =0.975. The shock profile is quite crisp, but the contact surface and the expansion wave is severely smeared due to the large dissipation (see Fig. 8). The Van Leer scheme has the maximum CFL=0.96, but the profile has a tail at the end of the expansion wave (see Fig. 9). The tail becomes shorter with decreasing CFL number and eventually disappear at CFL=0.45 [5]. The Roe scheme has the maximum CFL=0.945. Fig. 10 also shows the shock profile has oscillations when the CFL is greater than the maximum allowable CFL number with the value of 0.99. Zha scheme has the maximum allowable CFL=0.92. Among all the schemes tested, Zha scheme resolves the front of the expansion wave most accurately (located at about X/L=3.5). A tail at the end of the expansion will also appear for Zha scheme if the CFL is greater than 0.92. It is unexpected that the maximum allowable CFL number of AUSM$^+$ scheme is far below 0.9 with the value of 0.275. The whole profile is largely smeared due to the low CFL number used (see Fig. 12).

Table 1 summarizes the maximum allowable CFL number in the order of magnitude for each scheme.

3.2.2 Case 2: Slowly Moving Contact Surface

This is the case used in [12, 17] with the initial condition $[\rho, u, p]_L = [0.125, 0.112, 1.0]$, $[\rho, u, p]_R = [10.0, 0.112, 1.0]$. Fig. 13 shows that the schemes of LDFSS(2), AUSM$^+$, Roe

Table 1: Maximum CFL Numbers for Sod 1D Shock Tube

Scheme	CFL Number
Edwards LDFSS(2)	0.999
Van Leer-Hänel	0.99
Steger-Warming	0.975
Van Leer	0.96
Roe	0.945
Zha	0.92
Liou $AUSM^+$	0.275

and Zha can resolve the contact surface accurately as they are designed. The number of mesh points used is 201. The results of those schemes are at time level 0.02 and are virtually indistinguishable even though they have different maximum allowable CFL numbers. The velocity is uniformly constant and the density discontinuity is monotone. The Edwards LDFSS(2) scheme has far higher CFL number than the other schemes with the value of 0.97 while Zha scheme has 0.5, Liou's AUSM$^+$ has 0.48, and Roe scheme has the CFL value of 0.32.

The schemes of Van Leer, Van Leer-Hänel and Steger-Warming severely distort the profiles of the contact surfaces as shown in Fig. 14. The velocity profile are largely down and up. The density jumps are also seriously smeared.

Table 2 summarizes the maximum allowable CFL number in the order of magnitude for each scheme.

4 Conclusions

A numerical test case for the Euler equations is presented to examine the performance of several upwind schemes for satisfying the entropy condition. The first order upwind schemes of Roe, Van Leer, Steger-Warming, Van Leer-Hänel, Liou's AUSM and AUSM$^+$, Edwards's LDFSS and a modified Zha-Bilgen scheme are tested. The numerical test indicates that the Van Leer flux vector splitting scheme, Van Leer-Hänel and AUSM-type schemes do not satisfy the entropy condition and allow expansion shocks at sonic point when first order accurate discretizations are used. The schemes of Roe, AUSM, AUSM$^+$, and Van Leer-Hänel are not stable due to the presence of the expansion shocks. Van Leer scheme is stable, but yields a strong expansion shock. The flux vector splitting schemes of Steger-Warming and the modified Zha-Bilgen scheme yield a small jump at sonic point. The Edwards LDFSS(2) scheme gives the smoothest results at sonic point with a very small glitch when the coarse grid is used. Refined mesh decreases the non-smoothness of the Steger-Warming scheme, the modified Zha-Bilgen scheme and the Edwards LDFSS(2) scheme. When second order MUSCL interpolations are used, all the schemes obtain accurate results without any expansion shock and non-smoothness at sonic point. This may imply that using higher than first order spatial accuracy may generally avoid expansion shocks.

Table 2: Maximum CFL numbers of the schemes resolving the contact surface

Scheme	CFL Number
Edwards LDFSS(2)	0.97
Zha	0.5
Liou $AUSM^+$	0.48
Roe	0.32

Two shock tube problems, the Sod problem and a slowly moving contact discontinu-

ity, are also tested for these schemes. The schemes of Roe, Edwards' LDFSS(2), Liou's AUSM$^+$ and the modified Zha-Bilgen are able to resolve the contact discontinuity accurately. The Edwards LDFFS(2) scheme performs the best based on the maximum allowable CFL number and the profiles of shock and contact discontinuities.

References

[1] P. Roe, "Approximate Riemann Solvers, Parameter Vectors, and Difference Schemes," *Journal of Computational Physics*, vol. 43, pp. 357–372, 1981.

[2] B. Van Leer, "Flux-Vvector Splitting for the Euler Equations," *Lecture Note in Physics*, vol. 170, pp. 507–512, 1982.

[3] D. Hänel, R. Schwane, and G. Seider, "On the Accuracy of Upwind Schemes for the Solution of the Navier-Stokes Eqautions." AIAA paper 87-1105 CP, 1987.

[4] M.-S. Liou and C. J. Steffen, "A New Flux Splitting Scheme," *Journal of Computational Physics*, vol. 107, pp. 1–23, 1993.

[5] G.-C. Zha and E. Bilgen, "Numerical Solutions of Euler Equations by Using a New Flux Vector Splitting Scheme ," *International Journal for Numerical Methods in Fluids*, vol. 17, pp. 115–144, 1993.

[6] A. Jameson, "Analysis and Design of Numerical Schemes for Gas Dynamics I: Artificial Diffusion, Upwind Biasing, Limiters and Their Effect on Accuracy and Multigrid Convergence in Transonic and Hypersonic Flow." AIAA Paper 93-3359, July, 1993.

[7] A. Jameson, "Analysis and Design of Numerical Schemes for Gas Dynamics I: Artificial Diffusion, Upwind Biasing, Limiters and Their Effect on Accuracy and Multigrid Convergence in Transonic and Hypersonic Flow," *Journal of Computational Fluid Dynamics*, vol. 4, pp. 171–218, 1995.

[8] A. Jameson, "Analysis and Design of Numerical Schemes for Gas Dynamics II: Artificial Diffusion and Discrete Shock Structure," *Journal of Computational Fluid Dynamics*, vol. 5, pp. 1–38, 1995.

[9] M.-S. Liou, "Progress Towards an Improved CFD Methods: AUSM$^+$." AIAA Paper 95-1701-CP, June, 1995.

[10] M.-S. Liou, "A Sequel to AUSM: AUSM$^+$," *Journal of Computational Physics*, vol. 129, pp. 364–382, 1996.

[11] J. R. Edwards, "A Low-Diffusion Flux-Splitting Scheme for Navier-Stokes Calculations." AIAA Paper 95-1703-CP, June, 1995.

[12] J. R. Edwards, "A Low-Diffusion Flux-Splitting Scheme for Navier-Stokes Calculations," *Computer & Fluids*, vol. 6, pp. 635–659, 1997.

[13] S. Osher, "Numerical Solution of Singular Perturbation Problems and Hyperbolic Systems of Convervation Laws," *in Mathematics Studies*, vol. 47, pp. 179–205, 1981.

[14] A. Harten, P. D. Lax, and B. Van Leer, "On Upstream Differencing and Godunov-type Scheme for Hyperbolic Conservation Laws," *SIAM Review*, vol. 25, No.1, pp. 35–61, Jan. 1983.

[15] P. L. Roe, "Characteristic-Based Schemes for the Euler Equations," *Ann. Rev. Fluid Mech.*, vol. 18, pp. 337–65, 1986.

[16] J. Steger and R. Warming, "Flux Vvector Splitting of the Inviscid Gasdynamic Equations with Application to Finite-Difference Methods," *Journal of Computational Physics*, vol. 40, pp. 263–293, 1981.

[17] Y. Wada and M.-S. Liou, "An Accurate and Robust Splitting Scheme for Shock and Contact Discontinuities." AIAA Paper 94-0083, 1994.

[18] B. Van Leer, "On the Relation between the Upwind-Differencing Schemes of Godunov, Enguuist-Osher and Roe," *SIAM J. Sci. Stat. Comput.*, vol. 5, No. 1, pp. 1–20, 1984.

[19] M. L. Mason and L. E. Putnam, "The Effect of Throat Contouring on Two-Dimensional Converging-Diverging Nozzles at Static Conditions ." NASA Technical Paper 1704, 1980.

[20] V. L. Wells and R. A. Renaut, "Computing Aerodynamically Generated Noise," *Annual Review of Fluid Mechanics*, vol. 29, pp. pp. 161–199, 1997.

[21] G. Sod, "A survey of several finite difference methods for systems of nonlinear hyperbolic conversation laws," *Journal of Computational Physics*, vol. 27, pp. pp. 1–31, 1978.

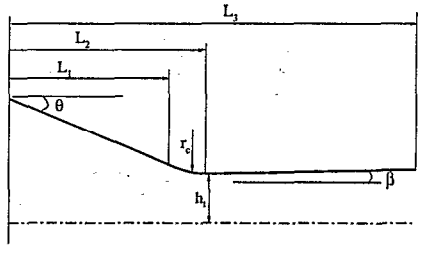

Figure 1: The sketch of Nozzle A2

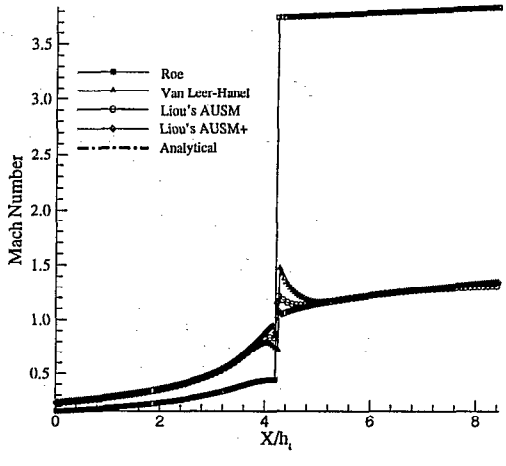

Figure 2: Mach number distributions computed using first order accuracy of different upwind schemes, 201 mesh points

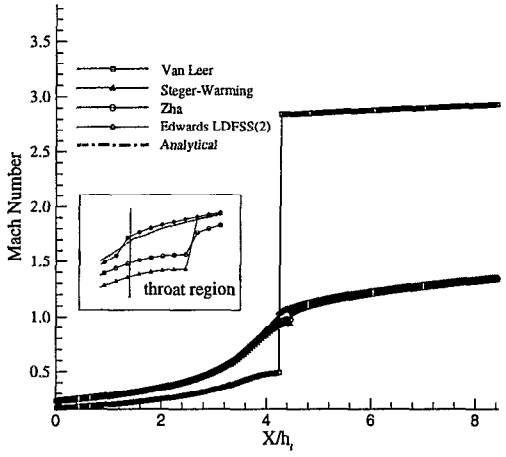

Figure 3: Mach number distributions computed using first order accuracy of different upwind schemes, 201 mesh points

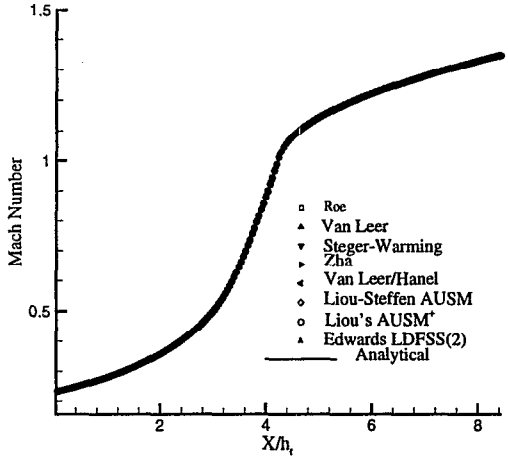

Figure 5: Mach number distributions computed using second order accuracy of different upwind schemes, 201 mesh points

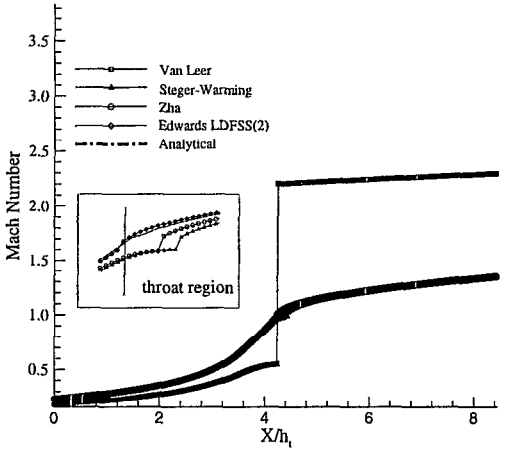

Figure 4: Mach number distributions computed using first order accuracy of different upwind schemes, 401 mesh points

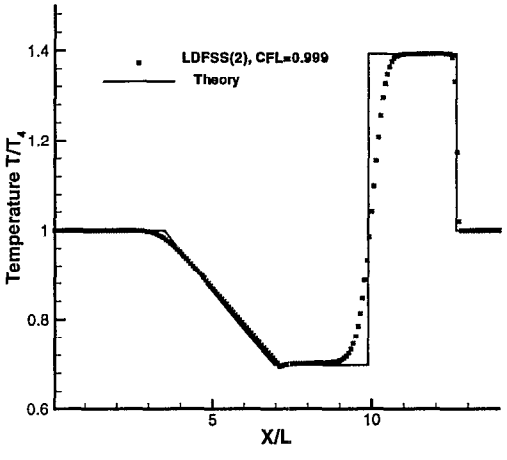

Figure 6: Temperature distribution computed by Edwrads LDFSS(2) scheme for Sod shock tube problem

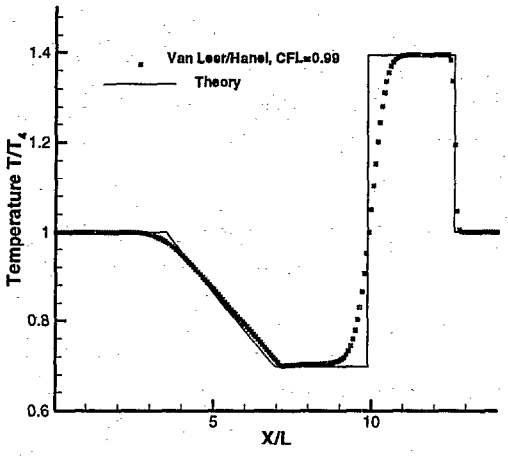

Figure 7: Temperature distribution computed by Van Leer-Hänel scheme for Sod shock tube problem

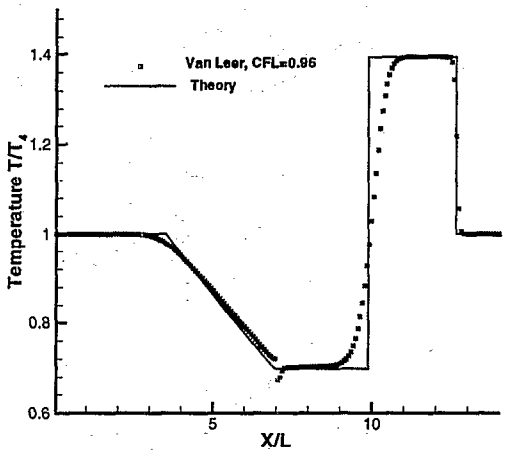

Figure 9: Temperature distribution computed by the Van Leer scheme for Sod shock tube problem

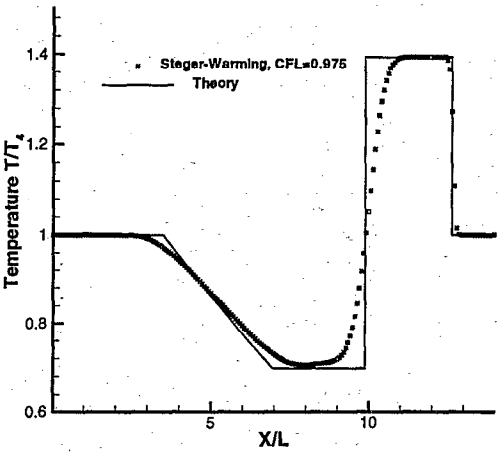

Figure 8: Temperature distribution computed by Steger-Warming scheme for Sod shock tube problem

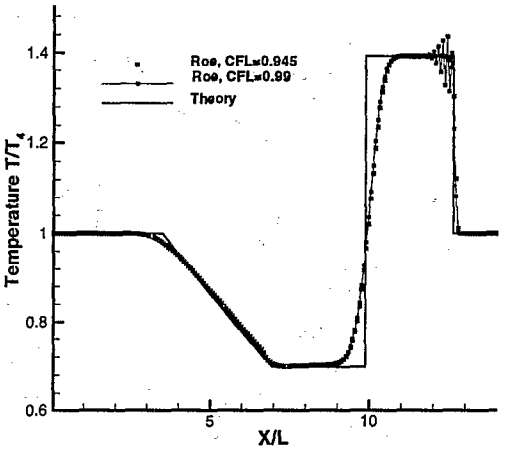

Figure 10: Temperature distribution computed by the Roe scheme for Sod shock tube problem

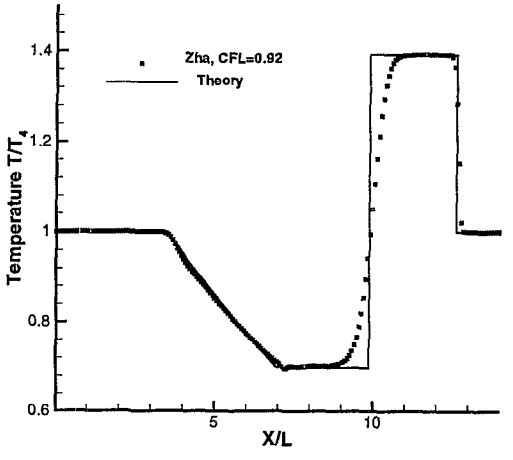

Figure 11: Temperature distribution computed by Zha scheme for Sod shock tube problem

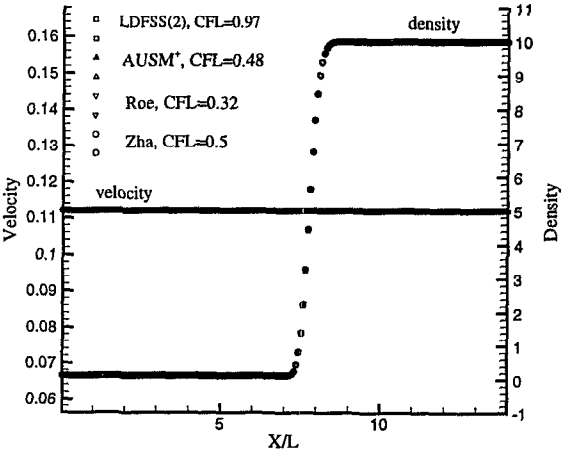

Figure 13: Computed velocity and density distributions for a slowly moving contact discontinuity

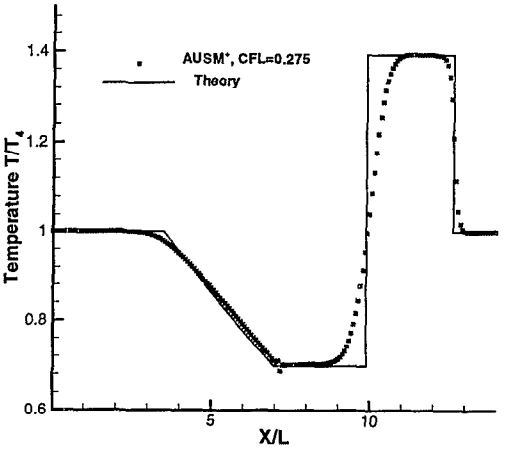

Figure 12: Temperature distribution computed by Liou's AUSM$^+$ scheme for Sod shock tube problem

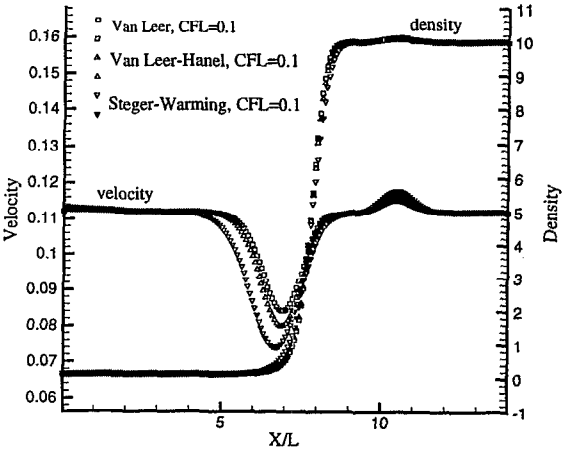

Figure 14: Computed velocity and density distributions using different upwind schemes for a slowly moving contact discontinuity